Optik 168 (2018) 342–347

Contents lists available at ScienceDirect

Optik

journal homepage: www.elsevier.de/ijleo

Original research article

Polarization-insensitive temperature sensor based on liquid filled photonic crystal fiber

Mohammad Abbasi, Mohammad Soroosh*, Ehsan Namjoo

Department of Electrical Engineering, Shahid Chamran University of Ahvaz, Iran

ARTICLE INFO

Article history:
Received 1 January 2018
Received in revised form 5 April 2018
Accepted 17 April 2018

Keywords:
Temperature sensor
Photonic crystal fiber
Liquid crystal
Optical confinement

ABSTRACT

In this paper, a polarization-insensitive temperature sensor based on photonic crystal fiber is proposed. Using finite element method, coupling between core and defected clad is analyzed. A high refractive index temperature sensitive liquid is infiltrated into the air holes of the second cladding ring. Numerical simulation shows as the phase matching between core and defect-clad super modes satisfied, resonance and peak confinement loss happen. A blue shift in resonance wavelength is obtained when temperature increases. Excellent linearity, simplicity and symmetrical structure, FOM of −0.272/°C and especially the same sensitivity of −1.96 nm/°C for both X and Y polarizations make the peak loss wavelength more detectable.

© 2018 Elsevier GmbH. All rights reserved.

1. Introduction

Photonic crystal fibers (PCFs) [1,2] have been widely used in accurate sensing of physical phenomena such as strain [3], refractive index [4,5], biological events [6], pressure [7], temperature, and so on. These sensors have unique advantages such as high sensitivity, good physical stability, immunity to electromagnetic wave, corrosion resistance, and great design flexibility compared with conventional fiber [8].

PCF temperature sensors with different structures and principles which are mostly based on the coupling or interfering between two guided modes have been widely studied in recent years. The operation phenomena relies on energy transfer between two modes. The phase matching and coupling condition of the guided modes has to be satisfied [9]. Fabry-Perot interferometric temperature sensors were proposed by Hu et al. [10] which are formed by just splicing a section of PCF with a single-mode fiber (SMF) showing the low response of 11.12 pm/°C (30–80 °C). Fiber Bragg grating (FBG) temperature sensors [11] have a very sharp reflection peak, but low sensitivity of −19.6 pm/°C.

Functionality of PCF temperature sensors can be improved using core doping, metal coating, infiltrations such as polymer and liquid into the air holes. PCF interferometer sensors with germanium doped fiber core [12] have a wide temperature range (0–500 °C) however they have low sensitivity of 78 pm/°C. Mach–Zehnder interferometer using a selectively polymer-filled two-core photonic crystal fiber, leads to a large thermo-optic mismatch between two cores and sensitivity of 1.595 nm/°C can be achieved [13]. Liquid or high refractive index liquid crystals (LCs) such as ethanol [14], chloroform, and nematic liquid crystals (NLCs) are good infiltration candidate due to their large thermo-optic coefficient and tuneability [15]. LC filled PCF temperature sensors [16–18] have different polarization sensitivities (1.7, 2.82 and 3.86 nm/°C for X polarization and 2.0, 1.99 and 5.5 nm/°C for Y polarization respectively). NLC filled PCF temperature sensors reported by Hu et al. [19] achieved

* Corresponding author.
E-mail address: m.soroosh@scu.ac.ir (M. Soroosh).

https://doi.org/10.1016/j.ijleo.2018.04.116
0030-4026/© 2018 Elsevier GmbH. All rights reserved.

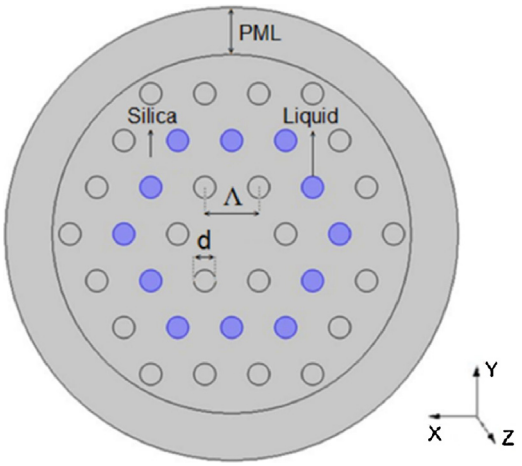

Fig. 1. Cross section of the PCF temperature sensor in XY plane.

good response of 3.90 nm/°C but the temperature detecting window was just 9/°C. PCF temperature sensor based on surface plasmon resonance coated with metal-sensitivity material such as gold [20] or filled with liquid and silver nanowire [21–23] have the different polarization sensitivity as well.

In this paper, at first a PCF temperature sensor will be designed based on complete coupling between core and defect-clad super modes. A large thermo-optic coefficient LC is supposed to be injected into the second cladding air hole ring of PCF. Then the sensor will be analyzed theoretically using the finite element method (FEM). Simulation results show that as the phase matching condition between core and defect-clad super modes is satisfied, resonance is obtained and the power in the transferring core couples to the defect core and the confinement losses increase remarkably. The sensitivity of both X and Y polarizations is −1.96 nm/°C and because the peak resonance for both X and Y polarizations happen approximately at the same wavelength, this sensor is very suitable for detecting the peak confinement loss. The proposed temperature sensor, shows excellent linearity, high figure of merit (FOM = −0.272/°C) with the temperature detecting window between 20 °C and 80 °C. The results shows a better performance compared with some similar proposed sensors. At the rest, the influence of changing some geometrical parameter such as the first ring cladding air hole size on the sensor functionality will be discussed.

2. Structure designed and simulation method

The cross section of the designed PCF temperature sensor in XY plane is shown in Fig. 1. The air holes are arranged in a triangular lattice. The pitch and the diameters of all air holes are Λ = 4 μm and d = 1.6 μm respectively.

The background material of the fiber is fused silica whose dispersion relationship corresponding to temperature is calculated by Sellmeier equation [24]:

$$n^2(\lambda, T) = \left(1.31552 + 6.90754 \times 10^{-6}T\right) + \frac{\left(0.788404 + 23.5835 \times 10^{-6}T\right)\lambda^2}{\lambda^2 - \left(0.0110199 + 0.584758 \times 10^{-6}T\right)} + \frac{\left(0.91316 + 0.548368 \times 10^{-6}T\right)\lambda^2}{\lambda^2 - 100} \quad (1)$$

where T is the temperature in Celsius, and λ is the free space wavelength in microns. A temperature sensitive liquid [16] with the refractive index of 1.65 at room temperature (25 °C) supposed to be filled into the air holes of the second cladding ring by capillary effect [8]. The refractive index of liquid between 20 °C and 80 °C can be expressed by:

$$n_{liq} = 1.65 - 4.65 \times 10^{-4}(T - 25) \quad (2)$$

where -4.65×10^{-4}/°C is the thermo-optic coefficient of liquid and T is the temperature in Celsius. The refractive index profile of silica and liquid as a function of temperature are shown in Fig. 2.

To investigate the influence of temperature on the PCF temperature sensor, the modal analysis in XY plane (while light propagation is along Z direction) was performed using Comsol Multiphysics software for different temperatures (20, 35, 50, 65, and 80 °C). To reduce the boundary reflections, anisotropic perfectly matched layers (PMLs) with absorbing boundary conditions are employed. The whole section of the sensor is divided into 10,520 triangular mesh elements. In order to determine the operating temperature, the real part of effective refractive index curve of core super mode and liquid-clad super mode as well as peak confinement loss when resonance between core and liquid-clad super mode happens will be extracted.

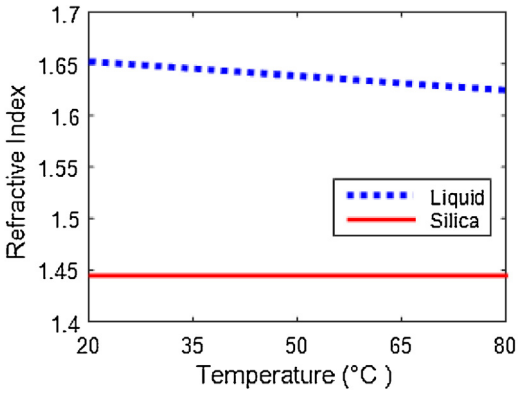

Fig. 2. The refractive index profile of silica and liquid as a function of temperature.

3. Simulation results and analysis

According to the simulation results, there are two pair super modes in the PCF which each pair consist of X and Y polarization super modes. From each pair, the X polarization super modes are selected and wavelength dependency of effective refractive index of these modes at the temperature of 50 °C is presented in Fig. 3(a).

One can see that at the shorter wavelength, the mode field of lower super mode is mainly distributed in silica-core and the mode field of higher super mode resides in liquid-clad region. As the wavelength increases, the electrical field of lower super mode starts transferring to the liquid-clad region and the mode transition is just contrary to that of the higher super mode. This is called complete coupling.

At the coupling wavelength and field transferring, a remarkable confinement loss is observed. Confinement loss which is the light confinement ability within the core region, for two super modes are presented in Fig. 3(b). The corresponding confinement loss of fiber expression is [24]:

$$\alpha(x, y) = 8.686 \times \frac{2\pi}{\lambda} \mathrm{Im}(n_{\mathrm{eff}}) \times 10^6 \tag{3}$$

where unit of the loss and wavelength are dB/m and μm, respectively, and Im(neff) represents the imaginary part of effective refractive index of super mode.

To explain the above qualitative descriptions, coupled-mode theory is very helpful. The equations for two modes which are supposed to be coupled are [5]:

$$\begin{cases} \dfrac{dE_1}{dz} = i\beta_1 E_1 + i\kappa E_2 \\ \dfrac{dE_2}{dz} = i\kappa E_1 + i\beta_2 E_2 \end{cases} \tag{4}$$

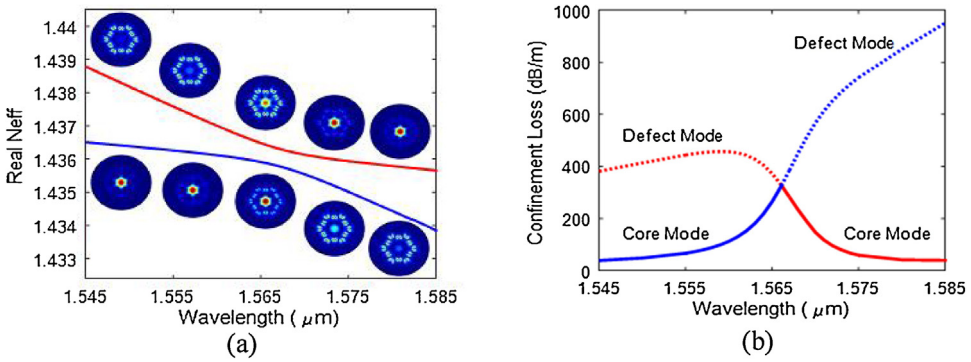

Fig. 3. (a) The real part of refractive index, and (b) confinement loss of X polarization super modes as a function of wavelength at the temperature of 50 °C.

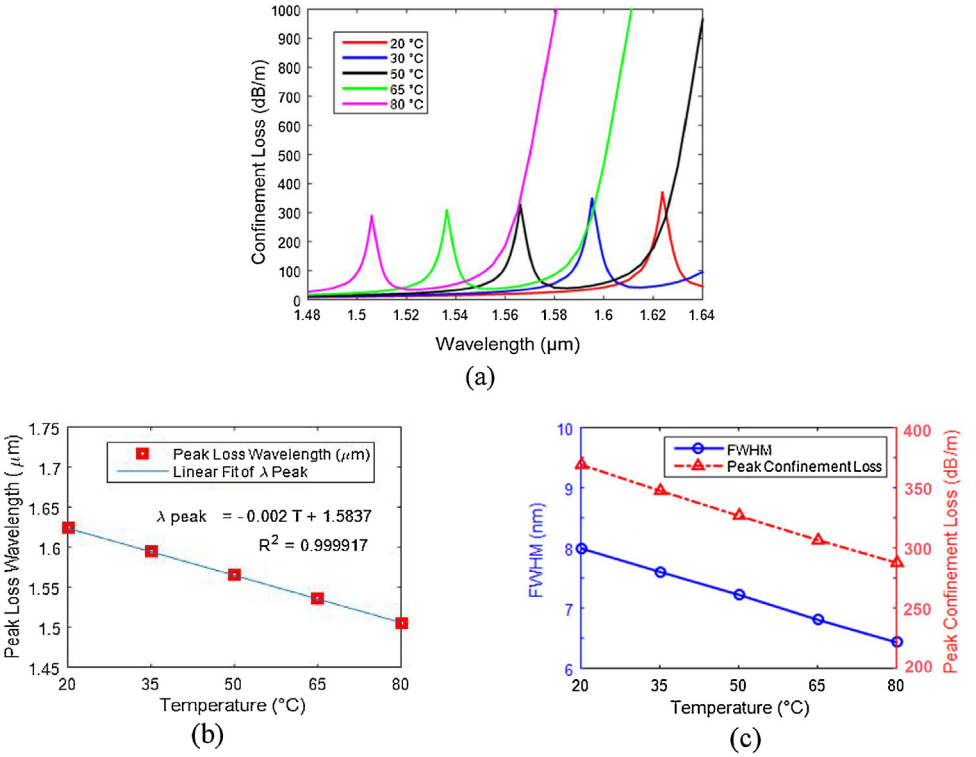

Fig. 4. (a) Confinement loss as a function of temperature, (b) dependency of the peak loss wavelength on temperature, and (c) FWHM and peak confinement loss versus temperature. (For interpretation of the references to colour in the text, the reader is referred to the web version of this article.)

where E_1 and E_2 are the mode fields of two coupling modes respectively, β_1 and β_2 are their propagation constants due to the waveguide geometry, and κ is the coupling strength. Assuming β as the propagation constant of the coupling mode, E_1 and E_2 could be written as $E_1 = A\exp(i\beta z)$ and $E_2 = B\exp(i\beta z)$. By substitution E_1 and E_2 in Eq. (4):

$$\begin{bmatrix} \beta-\beta_1 & -\kappa \\ -\kappa & \beta-\beta_2 \end{bmatrix} \begin{bmatrix} A \\ B \end{bmatrix} = 0 \tag{5}$$

By using the left expression det = 0, propagation constant of coupling mode β is calculated:

$$\beta_{\pm} = \beta_{ave} \pm \sqrt{\delta^2+\kappa^2} \tag{6}$$

where $\beta_{ave} = (\beta_1+\beta_2)/2$ and $\delta = (\beta_1-\beta_2)/2$. Because the real part of two super modes is lower than background material, these modes are leaky. β_1 and β_2 and as a result δ are complex. The real parts of the two leaky mode propagation constants are equal at phase matching point, so $\delta_r = 0$. It can be derived that when $\delta_i < \kappa$, β_+ and β_- have different real parts but equal imaginary parts and a complete coupling between two super modes happens. When δ_i is larger than κ, β_+ and β_- have equal real parts but different imaginary parts and an incomplete coupling appears. It is observed that the coupling and incomplete coupling condition depend on the coupling strength κ.

There is an intersection between loss curves of two super modes. At the intersection wavelength, both phase matching and loss matching conditions are satisfied and the resonant confinement loss peak is observed. Regarding Fig. 2, by increasing the temperature, refractive index of the filling liquid will be more decreased than silica because of the larger thermo-optic coefficient.

As Fig. 4(a) demonstrates, temperature increment leading the blue shift in peak loss wavelength. By measuring the peak loss wavelength shift, temperature changes can be detected effectively. The dashed red curve of Fig. 4(b) illustrates the effect of temperature on the peak loss. By increasing the temperature, the peak loss decreases. The relationship between peak loss wavelength and temperature is plotted in Fig. 4(b). The fitting curves can be expressed as $\lambda_{Peak} = -0.002\,T + 1.5837$ where λ is in micrometer and T is in Celsius. The correlations $R^2 = 0.999917$ between the fitting results with the simulation results shows an excellent linearity. Also according to Fig. 4(a), full width at half maximum (FWHM) and peak confinement loss are shown in Fig. 4(c).

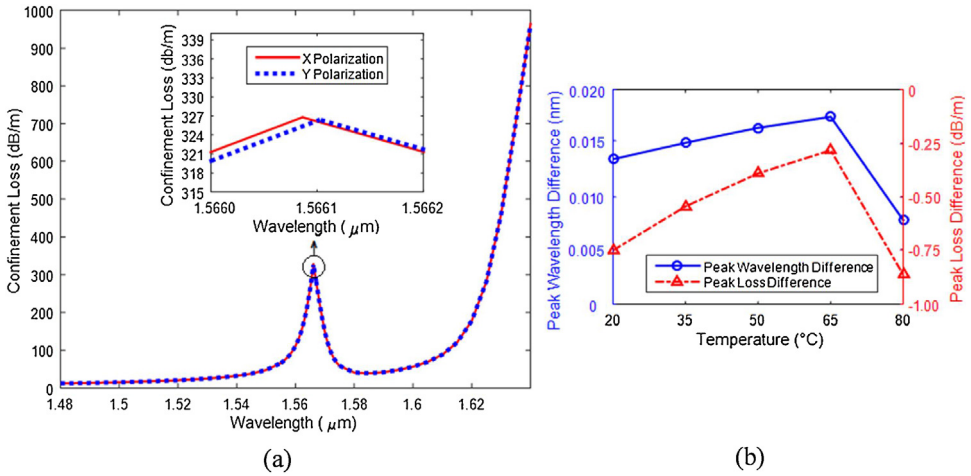

Fig. 5. (a) The confinement loss curves of both X and Y polarizations at the temperature of 50 °C, (b) the difference between peak wavelengths and losses for both X and Y polarizations in different temperatures. (For interpretation of the references to colour in the text, the reader is referred to the web version of this article.)

The wavelength sensitivity in terms of temperature is defined as [22]:

$$S\,[nm/^{\circ}] = \frac{d\lambda_{peak}(T)}{dT} \tag{7}$$

According to the simulation results, the mean temperature sensitivity is S = −1.96 nm/°C. The blue curve in Fig. 4(c) shows that the mean FWHM is equal to 7.2 nm. Figure of merit is calculated by [22]:

$$FOM\,[/^{\circ}] = \frac{S}{\mathrm{FWHM}} \tag{8}$$

The average FOM is −0.272/°C. The confinement loss curve of both X and Y polarizations at the temperature of 50 °C are presented in Fig. 5(a). As the blue curve of Fig. 5(b) shows, in all temperature, the difference between X and Y polarization peak loss wavelengths is less than 0.02 nm which could be neglected and leading to a more detectable peak loss in the real measurement application. The dashed red curve shows the difference between peak loss of X and Y polarizations in various temperature which is less than 1 dB/m. The simulation results show the same sensitivity, FWHM, and FOM for both X and Y polarizations.

The sensitivity of both X and Y polarizations S = −1.96 nm/°C is better than [10,11,13,21,23,24]. Our temperature sensor, showing excellent linearity better than [13,18,21,23,24], and high figure of merit (FOM = −0.272/°C) better than [23,24] and wider temperature detecting window (20–80 °C) better than [19,22,23].

The size of the first ring cladding air holes, plays a crucial role on coupling strength. By increasing the first ring cladding air hole size enough if $\delta_i < \kappa$ is still respected, complete coupling between super modes happens and the electric field of lower super mode transfers more rapidly to the liquid-clad region. The influence of diameter of the first ring cladding air hole on confinement loss is illustrated in Fig. 6(a). Blue and dashed red curves in Fig. 6(b) show FWHM and pick confinement loss respectively as a function of air hole diameter. It is clearly indicated by increasing the first ring cladding air hole size,

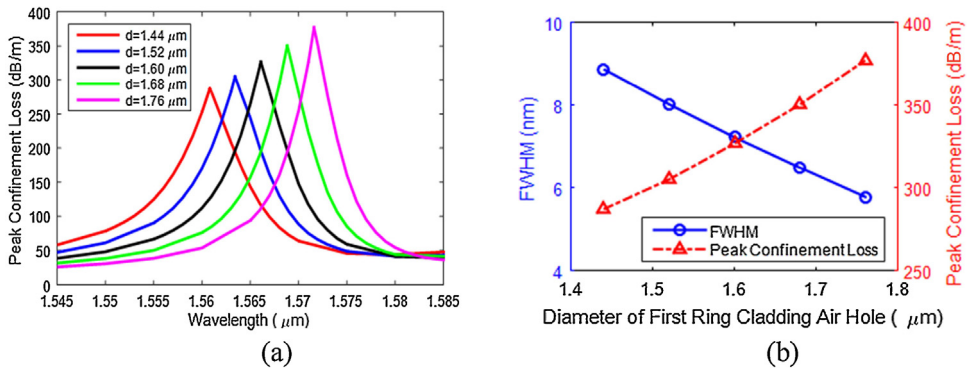

Fig. 6. (a) Peak confinement loss with different diameters of the first ring cladding air holes, (b) FWHM and pick confinement loss versus the first ring cladding air hole diameter. (For interpretation of the references to colour in the text, the reader is referred to the web version of this article.)

the peak loss will increase and FWHM becomes less which shows a better performance in the actual application. Very large air hole size leads to $\delta_i > \kappa$ and causes incomplete coupling between super modes and decreases the peak loss which is not suitable for detection and real application.

4. Conclusion

A temperature sensor based on photonic crystal fiber filled with temperature sensitive material was demonstrated in this paper. As the phase matching satisfies, complete coupling between core and liquid-clad super modes leads to confinement loss peak in the fiber. Temperature increment causes the blue shift in peak loss wavelength. The mean sensitivity, FWHM and FOM for both X and Y polarizations can reach to $-1.96\,nm/^{\circ}C$, 7.2 nm, and $-0.272/^{\circ}C$ respectively. By increasing the diameter of the first ring cladding air hole, performance characteristics will be enhanced. Regarding the simple structure, acceptable performance characteristics and because the peak resonance wavelength for both X and Y polarizations happens at the nearly same wavelength, this sensor is very suitable for the real temperature measuring applications.

References

[1] Ph. Russell, Photonic crystal fibers, Science 299 (2003) 358–362.
[2] B.J. Eggleton, C. Kerbage, P.S. Westbrook, R.S. Windeler, A. Hale, Microstructured optical fiber devices, Opt. Exp. 9 (2001) 698–713.
[3] L.M. Hu, C.C. Chan, X.Y. Dong, Y.P. Wang, P. Zu, W.C. Wong, W.W. Qian, T. Li, Photonic crystal fiber strain sensor based on modified Mach-Zehnder interferometer, IEEE Photon. J. 4 (2012) 114–118.
[4] J.L. Lim, D.J.J. Hu, P.P. Shum, Y. Wang, Cascaded photonic crystal fiber interferometers for refractive index sensing, IEEE Photon. J. 4 (2012) 1163–1169.
[5] Zh. Fan, Sh. Li, Q. Liu, G. An, H. Chen, J. Li, D. Chao, H. Li, J. Zi, W. Tian, High sensitivity of refractive index sensor based on analyte-filled photonic crystal fiber with surface plasmon resonance, IEEE Photon. J. 7 (2015) 4800809.
[6] L. Rindorf, J.B. Jensen, Photonic crystal fiber long-period gratings for biochemical sensing, Opt. Exp. 14 (2006) 8224–8231.
[7] Z. Ran, Sh. Liu, Q. Liu, Y. Wang, H. Bao, Y. Rao, Novel high-temperature fiber-optic pressure sensor based on etched PCF F-P interferometer micromachined by a 157-nm laser, IEEE Sens. J. 15 (2015) 3955–3958.
[8] Y. Wang, M. Yang, D.N. Wang, C.R. Liao, Selectively infiltrated photonic crystal fiber with ultrahigh temperature sensitivity, IEEE Technol. Lett. 23 (2011) 1520–1522.
[9] Zh. Zhang, Y. Shi, B. Bian, J. Lu, Dependence of leaky mode coupling on loss in photonic crystal fiber with hybrid cladding, Opt. Exp. 16 (2008) 1915–1922.
[10] F.X. Hu, X.H. Yang, W. Feng, J. Peng, F.G. Wei, B.W. Hong, Miniature Fabry-Perot interferometric sensor for temperature measurement based on photonic crystal fiber, Optoelec. Lett. 11 (2015) 0382–0385.
[11] R.C. Chaves, Ad.A.P. Pohl, I. Abe, R. Sebem, A. Paterno, Strain and temperature characterization of LPGs written by CO_2 laser in pure silica LMA photonic crystal fibers, Photon. Sens. 5 (2015) 241–250.
[12] F.C. Favero, M. Becker, R. Spittel, M. Rothhardt, J. Kobelke, H. Bartelt, Micro-structured fiber interferometer as sensitive temperature sensor, Photon. Sens. 3 (2013) 208–213.
[13] K. Naeem, B.H. Kim, B. Kim, Y. Chung, High-sensitivity temperature sensor based on a selectively-polymer-filled two-core photonic crystal fiber in-line interferometer, IEEE Sens. J. 15 (2015) 3998–4003.
[14] Y. Yu, X. Li, X. Hong, Y. Deng, K. Song, Y. Geng, H. Wei, W. Tong, Some features of the photonic crystal fiber temperature sensor with liquid ethanol filling, Opt. Exp. 18 (2010) 15383–15388.
[15] T.T. Larsen, A. Bjarklev, Optical devices based on liquid crystal photonic bandgap fibres, Opt. Exp. 11 (2003) 2589–2596.
[16] J. Du, Y. Liu, Zh. Wang, Zh. Liu, B. Zou, L. Jin, B. Liu, G. Kai, X. Dong, Thermally tunable dual-core photonic bandgap fiber based on the infusion of a temperature responsive liquid, Opt. Exp. 16 (2008) 4263–4269.
[17] Y. Peng, J. Hou, Y. Zhang, Z. Huang, R. Xiao, Q. Lu, Temperature sensing using the bandgap-like effect in a selectively liquid-filled photonic crystal fiber, Opt. Lett. 38 (2013) 263–265.
[18] H. Chen, Sh. Li, J. Li, Y. Han, Y. Wu, High sensitivity of temperature sensor based on ultracompact photonics crystal fibers, IEEE Photon. J. 6 (2014) 6803006.
[19] D.J.J. Hu, J.L. Lim, Y. Cui, K. Milenko, Y. Wang, P.P. Shum, T. Wolinski, Fabrication and characterization of a highly temperature sensitive device based on nematic liquid crystal-filled photonic crystal fiber, IEEE Photon. J. 4 (2012) 1248–1255.
[20] Y. Peng, J. Hou, Zh. Huang, Q. Lu, Temperature sensor based on surface plasmon resonance within selectively coated photonic crystal fiber, Appl. Opt. 51 (2012) 6361–6367.
[21] N. Luan, R. Wang, W. Lv, Y. Lu, J. Yao, Surface plasmon resonance temperature sensor based on photonic crystal fibers randomly filled with silver nanowires, Sensors 14 (2014) 16035–16045.
[22] Y. Lu, M.T. Wang, C.J. Hao, Z.Q. Zhao, J.Q. Yao, Temperature sensing using photonic crystal fiber filled with silver nanowires and liquid, IEEE Photon. J. 6 (2014) 6801307.
[23] X.C. Yang, Y. Lu, B.L. Liu, J.Q. Yao, Temperature sensor based on photonic crystal fiber filled with liquid and silver nanowires, IEEE Photon. J. 8 (2016) 6803309.
[24] Q. Liu, Sh. Li, H. Chen, Zh. Fan, J. Li, Photonic crystal fiber temperature sensor based on coupling between liquid-core mode and defect mode, IEEE Photon. J. 7 (2015) 4500509.